Journal of Applied Physics ARTICLE scitation.org/journal/jap

Doping induced charge density wave in monolayer TiS_2 and phonon-mediated superconductivity

Cite as: J. Appl. Phys. **127**, 044301 (2020); doi: 10.1063/1.5135615
Submitted: 7 November 2019 · Accepted: 5 January 2020 ·
Published Online: 22 January 2020

View Online Export Citation CrossMark

Ji-Hai Liao,[1,2] Yin-Chang Zhao,[3] Yu-Jun Zhao,[1,4] Xiao-Bao Yang,[1,4,a)] and Yue Chen[2,b)]

AFFILIATIONS

[1]Department of Physics, South China University of Technology, Guangzhou 510640, People's Republic of China
[2]Department of Mechanical Engineering, The University of Hong Kong, Pokfulam Road, Hong Kong SAR, China
[3]Department of Physics, Yantai University, Yantai 264005, People's Republic of China
[4]Key Laboratory of Advanced Energy Storage Materials of Guangdong Province, South China University of Technology, Guangzhou 510640, People's Republic of China

[a)]**Author to whom correspondence should be addressed:** scxbyang@scut.edu.cn
[b)]**Electronic mail:** yuechen@hku.hk

ABSTRACT

Using the first-principles calculations, we have investigated the effects of the charge doping and biaxial strain on the charge density wave (CDW) of monolayer octahedral titanium disulfide (1*T*-TiS_2). Our results show that proper electron doping can suppress the (2×2) CDW instability and the larger electron doping promotes a $(\sqrt{7} \times \sqrt{3})$ CDW phase involving a spontaneous breaking of the hexagonal crystal symmetry. Strain can affect the stability of doped monolayer 1*T*-TiS_2, but neither compressive strain nor tensile strain alone can stabilize the pristine one. When TiS_2 layers are decorated by metal atoms, such as Li, Na, K, Ca, and Al, the transferred charge can also suppress the (2×2) CDW instability. The stable doped 1*T*-TiS_2 is predicted to exhibit good phonon-mediated superconductivity, which can be further enhanced by strain. Our results reveal a unique CDW phenomenon in the electron-doped monolayer 1*T*-TiS_2 and that doping combined strain is efficient to modulate phonon softening, electron-phonon coupling, and superconductivity.

INTRODUCTION

Two-dimensional (2D) materials have attracted tremendous interest for their novel properties and potential applications.[1–10] Specifically, monolayers of transition metal dichalcogenides (TMDCs), which in bulk form are stacked by weak van der Waals force, are excellent candidates for device applications beyond graphene-based functional materials.[11–18] TiS_2 has drawn considerable attention because of the potential applications in batteries,[19–26] supercapattery,[27] and thermoelectric devices.[28–35] Recently, a monolayer form of octahedral TiS_2 (1*T*-TiS_2) has been isolated,[36–39] which prefers to form the (2×2) charge density wave (CDW) phase.[40] After many years of investigation, it is known that CDW may stem from electron-phonon coupling (EPC) or Fermi surface nesting, but there is not yet a universal theory that can explain all the observed CDWs.[41–45] CDW transitions in TMDCs are a common phenomenon and a vital and popular research topic.[46–51] CDWs in monolayer TMDCs are generally a planar projection of the corresponding bulk CDWs, such as 1*T*-TaS_2 (CDW: $\sqrt{13} \times \sqrt{13}$),[52,53] trigonal prismatic $NbSe_2$ (2*H*-$NbSe_2$) (3×3),[54,55] and 1*T*-$TiSe_2$ (2×2),[56] maintaining the symmetry of the hexagonal lattice. On the other hand, an unexpected $(\sqrt{7} \times \sqrt{3})$ CDW phase in which the hexagonal symmetry has been destroyed was observed in monolayer 1*T*-VSe_2.[57–59] Recently, (2×2) CDW phases of 1*T*-$TiTe_2$ were observed in epitaxial films at room temperature.[60] The CDW instability in monolayer 1*T*-$TiTe_2$ is similar to the phonon-mediated mechanism in 1*T*-$TiSe_2$.[56,61] Generally, TMDCs exhibit strong electron-phonon coupling (EPC); thus, superconducting and CDW states may coexist in bulk or monolayer form.[62–67] Remarkably, the transition between superconducting and CDW states in 2D TMDCs can be controlled by electron doping.[68]

In this paper, we have investigated the effects of the charge doping and biaxial strain on the CDW of monolayer 1*T*-TiS_2. Our results show that proper electron doping can suppress the (2×2) CDW instability and the larger electron doping promotes a unique $(\sqrt{7} \times \sqrt{3})$ CDW phase. We carefully studied the electron doping range before CDW transition happens. As decorated

by metal atoms, such as Li, Na, K, Ca, and Al, the accumulated charge on 1*T*-TiS_2 can also suppress the (2 × 2) CDW instability. The stable doped 1*T*-TiS_2 is predicted to exhibit good phonon-mediated superconductivity, which can be further enhanced by strain.

COMPUTATIONAL DETAILS

Our calculations were performed based on density functional theory (DFT) and density functional perturbation theory (DFPT) implemented in the QUANTUM-ESPRESSO package,[69] employing the projector augmented-wave (PAW) pseudopotentials[70] with the Perdew-Burke-Ernzerhof (PBE) exchange-correlation energy functional.[71] The plane-wave cutoff energies for wavefunctions and charge density were set to 60 Ry and 600 Ry, respectively. A vacuum region of 12 Å was adopted to avoid the interaction of the periodic images as the phonon spectra of monolayer 1*T*-TiS_2 and Na-intercalated bilayer 1*T*-TiS_2 have no remarkable difference from that at a vacuum of 20 Å (see Fig. S1 in the supplementary material). Of note, the vacuum thickness may affect the phonon frequency when charge is added/removed in the slab model as a uniform compensating background is required to maintain the charge neutrality (see Fig. S2 in the supplementary material). Therefore, the results obtained from the artificial charge doping in this work are qualitative. However, the vacuum thickness will not change the phonon frequency when 1*T*-TiS_2 is chemically doped as no charge compensating is necessary, and thus the results from chemical doping are quantitatively reliable. All the structures were fully relaxed until the Hellman-Feynman force on each atom was smaller than 10^{-5} Ry/Bohr. A Marzari-Vanderbilt cold smearing[72] of 0.02 Ry was used for the corresponding electronic self-consistent cycles. For calculations of electronic properties, a Monkhorst-Pack[73] k mesh of 24 × 24 × 1 was used. Phonon frequencies and EPC parameter λ were calculated with a phonon wave-vector mesh of 12 × 12 × 1 and a denser k mesh of 48 × 48 × 1, respectively.

RESULTS AND DISCUSSION

Figure 1(a) shows (2 × 2) and ($\sqrt{7} \times \sqrt{3}$) supercells, as well as the unitcell of monolayer 1*T*-TiS_2. The areas of the (2 × 2) and ($\sqrt{7} \times \sqrt{3}$) supercells are four and five times the area of the unitcell. The Brillouin zones of (2 × 2) and ($\sqrt{7} \times \sqrt{3}$) structures are shown in Figs. 1(b) and 1(c), comparing with that of unitcell. The optimized lattice constant of monolayer 1*T*-TiS_2 with the hexagonal crystal structure, $a = b$, is 3.41 Å, in good agreement with the experimentally observed ones, 3.40 Å[37] and 3.41 Å.[38] A previous study[40] has shown that the monolayer 1*T*-TiS_2 prefers to form (2 × 2) CDW phase than the normal phase because of a phonon mode with significant imaginary frequency at high symmetric point *M* in the Brillouin zone edges. The *M* points of the unitcell fold to Γ in the (2 × 2) supercell. Consequently, the system stabilizes by forming a (2 × 2) CDW phase with a distorted lattice (see Fig. S3 in the supplementary material).

A possibility for suppressing the CDW phase is by charge doping, as already suggested for monolayer 1*T*-$TiSe_2$, which also forms a (2 × 2) CDW phase at low temperature.[56,59,74] The imaginary phonon frequency at *M* moves up and then becomes real with increasing electron doping, indicating that the CDW instability in monolayer 1*T*-TiS_2 can be effectively suppressed via electron doping. The phonon frequencies are all positive when the concentration of doping is 0.2 electrons per formula unit (e/f.u.), as shown in Fig. 1(d). Interestingly, the phonon softening obviously appears at *S* and *T* in the high symmetric paths as the concentration of electron doping is 0.7 e/f.u. [see Fig. 1(e)]. The Kohn instability at *T* becomes a dynamical instability as the doping concentration further increases to 0.8 e/f.u. In the high symmetric paths, the lengths of $\overline{\Gamma T}$ and $\overline{MS}$ closely match 3/5 $\overline{\Gamma K}$ and $\overline{MK}$, respectively. The *T* and *S* in the Brillouin zone of the unitcell fold to Γ in the ($\sqrt{7} \times \sqrt{3}$) supercell, which is precisely the condition for the formation of a ($\sqrt{7} \times \sqrt{3}$) CDW structure. The number of valence electrons in the 1*T*-TiS_2 with high doping concentration is close to that of VS_2 and VSe_2. Recently, a ($\sqrt{7} \times \sqrt{3}$) CDW phase has been observed in monolayer 1*T*-VSe_2.[57] Monolayer 1*H*-VS_2 also tends to form a ($\sqrt{7} \times \sqrt{3}$) CDW phase, whereas monolayer 1*T*-VS_2 tends to form a ($\sqrt{21} \times \sqrt{3}$) CDW phase.[75] This indicates that the formation of CDW in TMDC is complicated. Considering the stability of CDW phase from an energy perspective, we defined the CDW formation energy as

$$\Delta E = E_{\mathrm{CDW}} - E_{1T}, \tag{1}$$

where E_{CDW} and E_{1T} are the total energies of the relaxed CDW phase and the normal phase, respectively. The results are shown in Fig. 2(a). The (2 × 2) CDW phase is 0.79 meV/f.u. lower than the undistorted and undoped 1*T*-TiS_2, in line with the previous local density approximation (LDA) value of 0.85 meV/f.u.[40] The phase transition from a (2 × 2) CDW phase to normal phase occurs at a doping concentration between 0.1 and 0.2 e/f.u. Increasing the doping concentration to 0.8 e/f.u., the total energy of the ($\sqrt{7} \times \sqrt{3}$) CDW phase is 0.08 meV/f.u. lower than that of the normal phase. The ($\sqrt{7} \times \sqrt{3}$) CDW distorted structure is shown in Fig. 2(b), where five Ti atoms aggregate to form a V shape with a maximum displacement of 0.06 Å, which is similar to the displacement of Ti atoms in the (2 × 2) CDW phase. Another displacement in the ($\sqrt{7} \times \sqrt{3}$) CDW distorted structure, which involves two Ti atoms in the middle of the V shape, is slightly larger than 0.02 Å. The symmetry of the ($\sqrt{7} \times \sqrt{3}$) CDW distorted structure is lowered down to *Cm* (No. 8) from $P\bar{3}m1$ (No. 164); nevertheless, that of (2 × 2) CDW is *P*321 (No. 150).

In order to obtain the critical doping concentration of the phase transition, we carefully calculated the phonon frequency at *M* and *T* at various concentrations under the condition of a vacuum layer of 12 Å. The minimum phonon frequencies at *M* and *T* are summarized in Fig. 1(f). A vital issue is that when the minimum phonon frequency at *M* or *T* approaches zero. One critical point is at the doping of 0.11 e/f.u., corresponding for the phase transition from a (2 × 2) CDW phase to the normal phase. The other is at 0.75 e/f.u. for the normal phase to the ($\sqrt{7} \times \sqrt{3}$) CDW phase transition. Note that the lattice constant of electron-doped monolayer TiS_2 expands, compared to the pristine one. The extent of lattice distortion Δ is defined as $\Delta = (a'/a - 1) \times 100\%$, where a' and a are the fully relaxed lattice constants of doped and undoped monolayer 1*T*-TiS_2, respectively. If the lattice parameters are fixed to the undoped structure, the doped ones are under biaxial strain. We define the biaxial strain ε as $\varepsilon = (a''/a' - 1) \times 100\%$, where a'' is a pre-set lattice constant. The calculated results show that the extent of

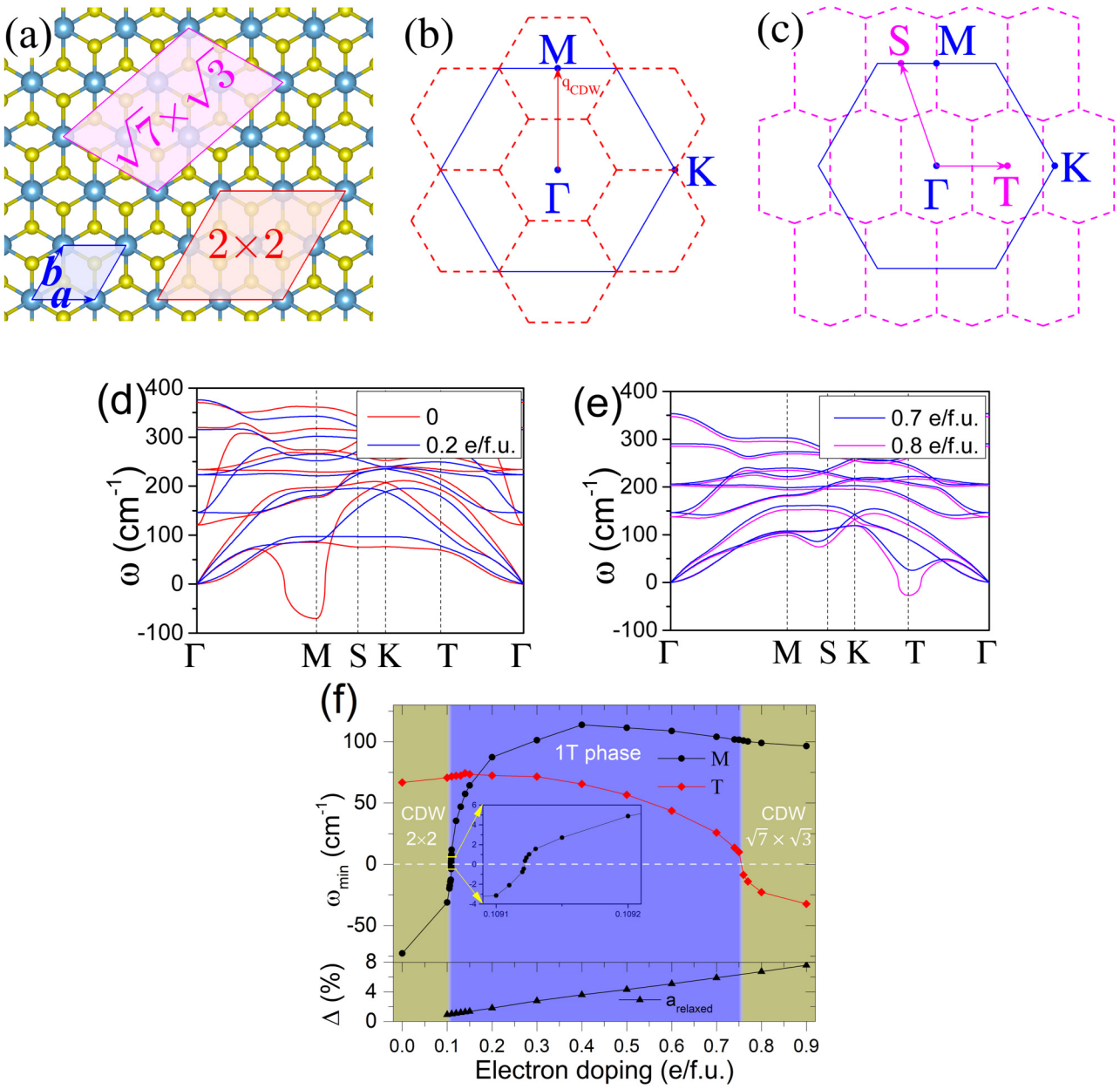

FIG. 1. (a) Top view of the atomic structure of monolayer 1*T*-TiS_2. *a* and *b* are the lattice constants of unitcell. (2 × 2) and ($\sqrt{7} \times \sqrt{3}$) supercells are shown in red rhombus and magenta parallelogram, respectively. The big blue and small yellow spheres represent Ti and S atoms, respectively. (b) Brillouin zones of the (1 × 1) and (2 × 2) structures are outlined in blue solid and red dash lines, respectively. (c) Brillouin zones of the (1 × 1) and ($\sqrt{7} \times \sqrt{3}$) structures are outlined in blue solid and magenta dash lines, respectively. (d) The phonon dispersions of pristine monolayer TiS_2 and doped TiS_2 with 0.2 e/f.u. (e) The phonon dispersions of doped TiS_2 with 0.7 and 0.8 e/f.u. (f) The minimum phonon frequency at *M* point and *T* point and the lattice distortion (Δ) as a function of electron doping under the condition of a vacuum layer of 12 Å. The area, 0.1091–0.1092 e/f.u. on the horizontal axis and −4 to 6 cm^{-1} on the vertical axis, is enlarged in the inset.

lattice distortion increases almost linearly with the increase of electron doping when the systems are fully relaxed [see the lower part of Fig. 1(f)]. For example, the lattice constant expands to $a' = 3.56$ Å with $\Delta = 4.3\%$ when the doping concentration is 0.5 e/f.u. Strain may be a potential way to suppress the CDW phase, as in monolayer 1*T*-$TiSe_2$. Unfortunately, neither compressive nor tensile strains alone can stabilize the pristine monolayer 1*T*-TiS_2 (see Fig. S4 in the supplementary material).

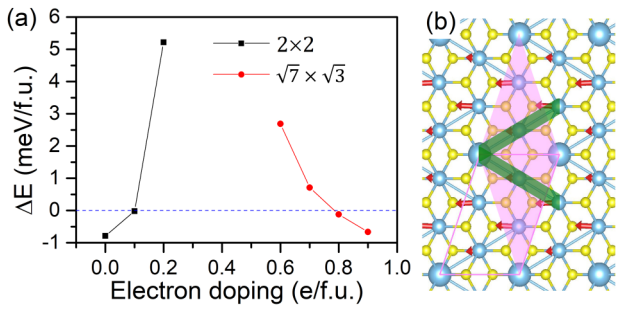

FIG. 2. (a) CDW formation energy ΔE per formula unit as a function of electron doping. (b) Top view of the atomic structure of the $(\sqrt{7}\times\sqrt{3})$ CDW phase. The supercell is outlined in magenta parallelogram as well as filled light magenta rhombus. The red arrows display the displacement directions and scales of the Ti atoms from the high symmetric positions of the pristine 1*T* structure. The Ti atoms that are stationary at the origin are enlarged.

Superconductivity can be induced in 1*T*-TiS_2 when the CDW phase is suppressed. Here, we estimate the T_c by using the McMillan–Allen–Dynes parameterized Eliashberg equation,[76]

$$T_c = \frac{\omega_{\log}}{1.2}\exp\left(-\frac{1.04(1+\lambda)}{\lambda-\mu^*(1+0.62\lambda)}\right), \tag{2}$$

where $\omega_{\log}$ is the logarithmic averaged phonon frequency

$$\omega_{\log} = \exp\left(\frac{2}{\lambda}\int\frac{\alpha^2F(\omega)\log(\omega)}{\omega}d\omega\right), \tag{3}$$

and λ is the total electron-phonon coupling constant

$$\lambda = \sum_{\mathbf{q}\nu}\lambda_{\mathbf{q}\nu} = 2\int\frac{\alpha^2F(\omega)}{\omega}d\omega. \tag{4}$$

In Eq. (3), $\alpha^2F(\omega)$ is the Eliashberg spectral function, which is defined as

$$\alpha^2F(\omega) = \frac{1}{2\pi N(E_F)}\sum_{\mathbf{q}\nu}\delta(\omega-\omega_{\mathbf{q}\nu})\frac{\gamma_{\mathbf{q}\nu}}{\hbar\omega_{\mathbf{q}\nu}}. \tag{5}$$

Here, $N(E_F)$ is the electronic density of states at the Fermi level, and the Dirac δ function is simulated by a Gaussian function. $\gamma_{\mathbf{q}\nu}$ is the linewidth of the phonon mode ν at a wave vector $\mathbf{q}$,

$$\gamma_{\mathbf{q}\nu} = 2\pi\omega_{\mathbf{q}\nu}\sum_{i,j}\int\frac{|g_{\mathbf{q}\nu}(\mathbf{k},i,j)|^2\delta(e_{\mathbf{q},i}-e_F)\delta(e_{\mathbf{k}+\mathbf{q},i}-e_F)}{\Omega_{BZ}}d^3k. \tag{6}$$

Ω_{BZ} is the volume of the first Brillouin zone. $g_{\mathbf{q}\nu}(\mathbf{k},i,j)$ is the EPC matrix element for scattering an electron from a Bloch state $i\mathbf{q}$ to another state $j\mathbf{q}+\mathbf{k}$, which is given by

$$g_{\mathbf{q}\nu}(\mathbf{k},i,j) = \sqrt{\frac{\hbar}{2M\omega_{\mathbf{q}\nu}}}\langle\psi_{i,\mathbf{k}}|dV/d\mathbf{u}_{\mathbf{q}\nu}|\psi_{j,\mathbf{k}+\mathbf{q}}\rangle, \tag{7}$$

where V is the Kohn–Sham potential, and $\mathbf{u}_{\mathbf{q}\nu}$ is the atomic displacement.

Following previous studies,[77–83] we use the Coulomb repulsion pseudopotential $\mu^*=0.1$ in this paper.

The calculated T_c for doped 1*T*-TiS_2 is shown in Fig. 3(a). The relation between T_c and electron doping is close to an up-parabola. The two ends of the curve show high T_c, and the corresponding minimum phonon frequencies ω at M and T are small positive values approaching zero [see the upper part of Fig. 1(f)]. An infinitesimal positive ω in Eq. (4) can lead to a large λ, resulting in high T_c. The relation between λ and electron doping is also close to an up-parabola, whereas that between $\omega_{\log}$ and electron doping is of down-parabola (see Fig. S5 in the supplementary material). The superconducting T_c is below 1 K at doping concentrations ranging from 0.13 to 0.5 e/f.u. because of the hardening phonon spectra. When a compressive strain of 2.0% is applied, T_c increases by more than six times to 6.65 K at a doping of 0.13 e/f.u., indicating that T_c is sensitive to lattice strain. At a doping of 0.5 e/f.u., T_c increases by more than three times to 3.59 K when a tensile strain of 1.5% is applied, where the lattice constants of the strained system are equal to those at the doping concentration of 0.7 e/f.u. with full relaxation. At a doping level of 0.5 e/f.u., we observe a noticeable phonon softening at T [see Fig. 3(b)]. The phonon softening is further enhanced when tensile strain is applied or electron doping concentration becomes higher, and the corresponding phonon linewidth increases, resulting in a larger λ [see Figs. 3(c) and 3(d)]. Moreover, as shown in the inset of Fig. 3(a), at a doping level of 0.5 e/f.u., the electronic density of states at the Fermi level monotonically increases with lattice expansion, leading to a monotonically increasing T_c.

The CDW instability in monolayer 1*T*-TiS_2 can also be effectively suppressed via hole doping (see Fig. S6 in the supplementary material). Imaginary phonon frequency is removed as the concentration of doping is 0.03 holes per formula unit (h/f.u.). T_c decreases sharply from 7.10 K to 0 as the doping concentration increases to 0.1 h/f.u. (see Fig. S7 in the supplementary material). In order to realize the chemical hole doping in 1*T*-TiS_2, F- and Cl-intercalated bilayer TiS_2 were considered. However, these structures are dynamically unstable (see Figs. S8 and S9 in the supplementary material).

Fortunately, electron doping can be realized by chemical doping. We primarily focused on two types of chemical doping. One is metal-intercalated bilayer 1*T*-TiS_2, denoted as $M(TiS_2)_2$ (M = Li, Na, K, Ca, or Al); the other is metal-deposited monolayer 1*T*-TiS_2, denoted as $MTiS_2$. For $M(TiS_2)_2$, we considered two configurations with stacking orders of CBACABC and ABCBABC [see Figs. 4(a) and 4(b)]. For instance, the phonon spectra, total energies, and T_c of $Na(TiS_2)_2$ with two different stacking orders are almost identical (see Fig. S10 in the supplementary material). The symmetry of the CBACABC configuration is higher than that of the ABCBABC configuration. Consequently, the computational cost of the CBACABC configuration is much lower than that of the ABCBABC configuration. For $MTiS_2$, the configuration with stacking order of CABC [see Fig. 4(c)] is more energetically stable than those of AABC and BABC. The following results are based on the configurations with stacking orders of CBACABC and CABC.

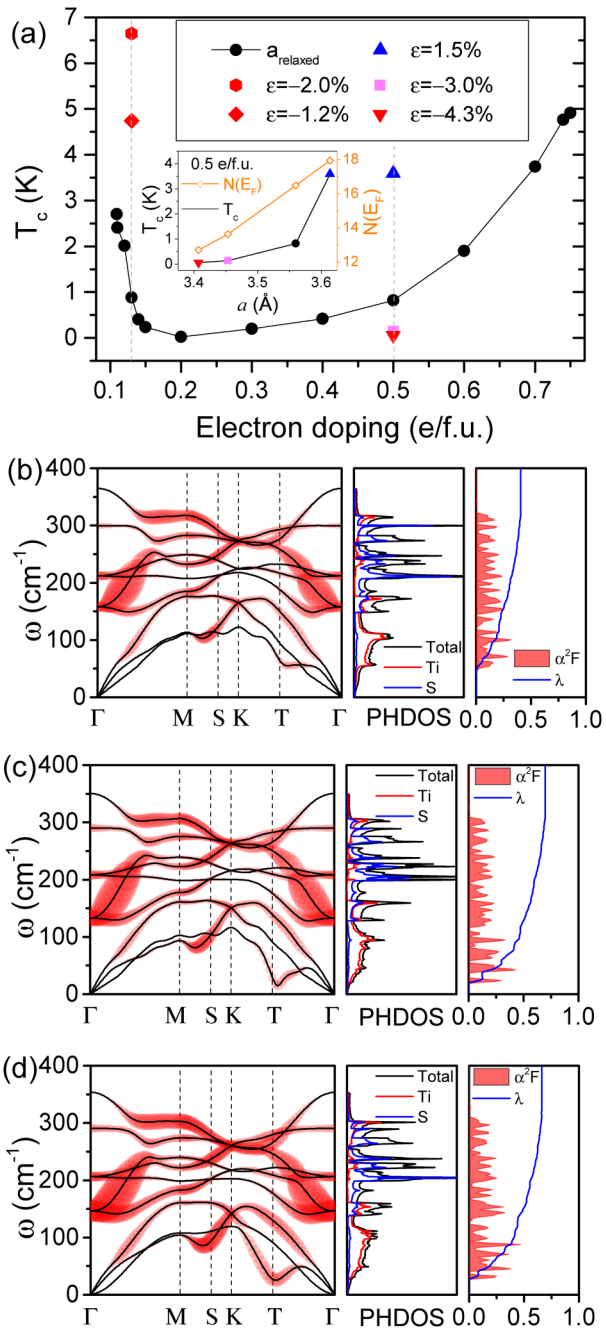

FIG. 3. (a) Calculated superconducting transition temperature (T_c) of monolayer TiS_2 as a function of electron doping with full relaxation (denoted as $a_{relaxed}$) or equibiaxial strain. Lattice dependent T_c and $N(E_F)$ at the doping level of 0.5 e/f.u. are shown in the inset. Phonon dispersion with phonon linewidth γ_{qv}, phonon density of states (PHDOS), and Eliashberg function $\alpha^2F(\omega)$ with $\lambda(\omega)$ for monolayer TiS_2 at a doping level of (b) 0.5 e/f.u. with full relaxation, (c) 0.5 e/f.u. with a lattice strain of 1.5%, and (d) 0.7 e/f.u. with full relaxation. The lattice constant of monolayer TiS_2 at a doping level of 0.5 e/f.u. with a lattice strain of 1.5% and that of 0.7 e/f.u. with full relaxation are equal to each other.

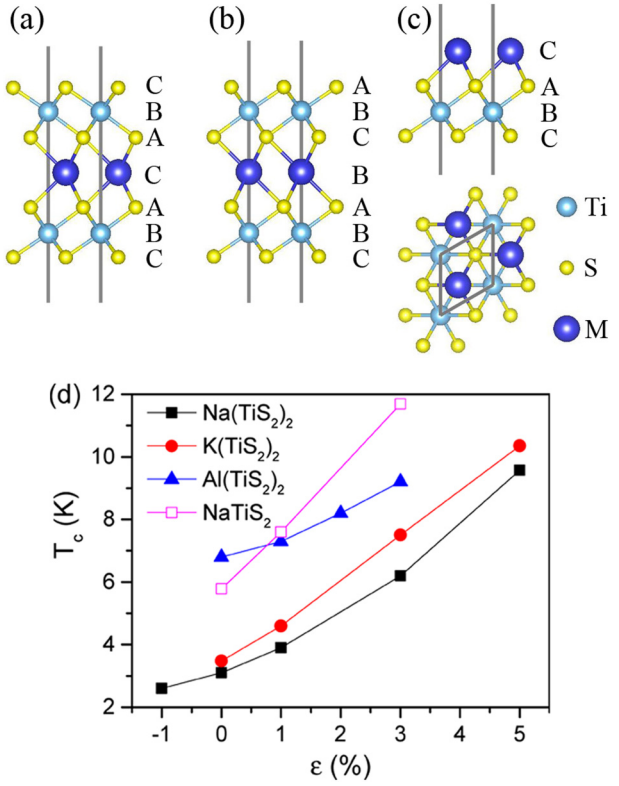

FIG. 4. Side views of the atomic structures of M-intercalated bilayer TiS_2 with stacking orders of (a) CBACABC and (b) ABCBABC. (c) Side and top views of the atomic structure of M-deposited monolayer TiS_2 with stacking order of CABC. (d) Superconducting transition temperature T_c as a function of biaxial lattice strain ε for $NaTiS_2$ and Na-, K-, and Al-intercalated bilayer TiS_2 (CBACABC).

Table I summarizes the lattice constant, electron doping concentration, EPC constant, and T_c of $M(TiS_2)_2$ and $MTiS_2$. The lattice constants expand when the systems are intercalated or deposited by Li, Na, K, or Ca. The lattice constants of $Al(TiS_2)_2$ and $AlTiS_2$ become smaller than that of 1T-TiS_2 due to the shortest Al nearest neighbor distance (2.86 Å) among these bulk metals. The quantitative analysis of electron doping was done by Bader charge population analysis.[84] Each TiS_2 is doped by 0.44 e, 0.40 e, or 0.38 e as Li, Na, or K intercalates bilayer TiS_2. $LiTiS_2$ becomes dynamically unstable due to the high doping concentration of 0.82 e/f.u. $Ca(TiS_2)_2$ is also dynamically unstable perhaps because Ca atoms donate too many electrons (1.32 e per Ca atom). Importantly, $CaTiS_2$, where the charge transition from Ca to TiS_2 is 0.79 e, is dynamically stable with the lattice constant expanding by 5.07%. Consequently, T_c of $CaTiS_2$ reaches 9.59 K. Tensile strain can enhance T_c of these systems on the condition that the structures remain dynamically stable [see Fig. 4(d)]. $CaTiS_2$ cannot bear a tensile strain of 1%, whereas $NaTiS_2$ and $Na(TiS_2)_2$ can bear strains of 3% and 5%, respectively. Table II provides the calculated values of $N(E_F)$, λ, ω_{log}, and T_c at maximum strain. As for Na

TABLE I. Calculated values of lattice constant a, lattice distortion Δ, electron doping to TiS_2 from the metal atoms, $N(E_F)$, λ, ω_{log}, and T_c. T_c was calculated using the McMillan–Allen–Dynes formula with $\mu^* = 0.1$.

	a (Å)	Δ (%)	Electron doping (e/TiS_2)	$N(E_F)$ (per cell)	λ	ω_{log} (K)	$T_c^{\mu^*=0.1}$ (K)
$Li(TiS_2)_2$	3.43	0.55	0.44	24.73	0.50	207.28	2.48
$Na(TiS_2)_2$	3.47	1.73	0.40	27.01	0.53	205.22	3.10
$K(TiS_2)_2$	3.52	3.08	0.38	29.23	0.55	200.96	3.48
$Ca(TiS_2)_2$	3.56	4.34	0.66	…	…	…	…
$Al(TiS_2)_2$	3.39	−0.60	0.78	30.21	0.70	197.33	6.80
$LiTiS_2$	3.54	3.74	0.82	…	…	…	…
$NaTiS_2$	3.48	2.05	0.55	18.06	0.70	166.41	5.78
$KTiS_2$	3.59	5.07	0.46	21.64	0.82	144.76	7.12
$CaTiS_2$	3.58	4.76	0.79	21.70	1.78	72.60	9.59
$AlTiS_2$	3.34	−2.16	0.80	…	…	…	…

TABLE II. Calculated values of $N(E_F)$, λ, ω_{log}, and T_c at certain biaxial strains ε. T_c was obtained with $\mu^* = 0.1$. The corresponding lattice constants a are also given.

	a (Å)	ε (%)	$N(E_F)$ (per cell)	λ	ω_{log} (K)	$T_c^{\mu^*=0.1}$ (K)
$Na(TiS_2)_2$	3.65	5	37.74	1.06	126.46	9.57
$K(TiS_2)_2$	3.69	5	39.95	1.42	95.95	10.38
$Al(TiS_2)_2$	3.49	3	35.20	0.94	146.18	9.21
$NaTiS_2$	3.59	3	23.30	1.50	102.26	11.69

$(TiS_2)_2$, the phonon softening at T point enhances gradually with increasing strain, and the system becomes dynamically unstable as strain reaches 6% (see Fig. S11 in the supplementary material), indicating that tensile strain can lead to a $(\sqrt{7} \times \sqrt{3})$ CDW phase transition. The highest T_c of $Na(TiS_2)_2$ with 5% strain and $NaTiS_2$ with 3% strain are 9.57 K and 11.69 K, respectively. There are phonon softening at T and S points for these two systems [see Figs. 5(a) and 5(b)]. The main contribution to EPC comes from the low-frequency phonons. Around each M point, there are two ellipses in the Fermi surface of unstrained $Na(TiS_2)_2$ [see Fig. S12(b) in the supplementary material]. Four electronic bands around Γ pass through the Fermi level at 5% strain (see Fig. S13 in the supplementary material). Consequently, four Γ-centered pockets appear on the Fermi surface of $Na(TiS_2)_2$ at 5% strain [see Fig. 5(c)], and the electronic density of states at the Fermi level increases significantly. The distribution of EPC constant $\lambda_{\mathbf{q}}$ in $\mathbf{q}$ space looks like a six-tooth gear, and the strongest EPC in $\mathbf{q}$ space is at T point under a strain of 5% [see Fig. 5(d)]. The Fermi surfaces of $NaTiS_2$ without and with a 3% strain have no remarkable difference [see Fig. 5(e) and Fig. S14(b) in the supplementary material], both showing a K-centered rounded triangle pocket. The nesting is obvious with nesting vectors $\mathbf{q}_1$, $\mathbf{q}_2$, and $\mathbf{q}_3$. The band structures of $NaTiS_2$ show that the band near the Fermi energy becomes less dispersive at a 3% strain compared to that of the unstrained one (see Fig. S15 in the supplementary material). Therefore, the electronic density of states of $NaTiS_2$ at the Fermi level also increases significantly under tensile strains. The EPC constant λ of $NaTiS_2$ at a 3% strain is twice greater than that of the unstrained one. The strongest EPC in $\mathbf{q}$ space is in a Γ-centered circle ring [see Fig. 5(f)]. These Fermi surfaces are

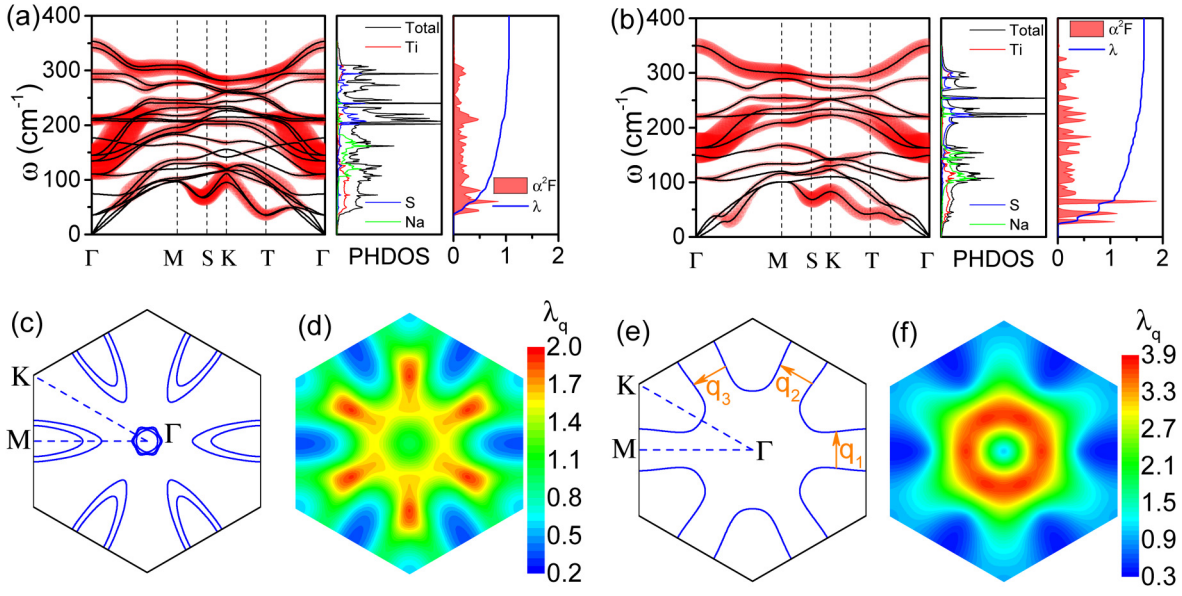

FIG. 5. Phonon dispersion with phonon linewidth $\gamma_{\mathbf{q}\nu}$, phonon density of states, and Eliashberg function $\alpha^2F(\omega)$ with $\lambda(\omega)$ for (a) $Na(TiS_2)_2$ under a biaxial strain of 5% and (b) $NaTiS_2$ under a biaxial strain of 3%. (c) Fermi surface and (d) distribution of EPC constant $\lambda_{\mathbf{q}}$ in $\mathbf{q}$ space for $Na(TiS_2)_2$ under a biaxial strain of 5%. (e) Fermi surface and (f) distribution of EPC constant $\lambda_{\mathbf{q}}$ in $\mathbf{q}$ space for $NaTiS_2$ under a biaxial strain of 3%.

mainly contributed by Ti-*d* orbitals. The Na-*s* orbitals do not contribute to $Na(TiS_2)_2$ but contribute about 20% to $NaTiS_2$ (see Fig. S16 in the supplementary material).

We also considered Na-decorated 2D 1*T*-TiS_2 in (2×2) supercells, denoted as $Na(TiS_2)_4$ and $Na(TiS_2)_8$ (see Figs. S17 and S18 in the supplementary material). There are slight distortions in these two configurations after full relaxation. Limited phonons are found to have imaginary frequency around Γ for $Na(TiS_2)_4$, whereas phonons across the whole Brillouin zone show imaginary frequency in $Na(TiS_2)_8$ (see Figs. S19 and S20 in the supplementary material). The calculated EPC constant of $Na(TiS_2)_4$ is 0.29. Each unit of TiS_2 is doped by 0.21 electrons in $Na(TiS_2)_4$; thus, this result is in line with the EPC constant variation of monolayer 1*T*-TiS_2 as a function of electron doping (see Fig. S5 in the supplementary material).

CONCLUSION

In summary, we have performed DFT calculations to investigate the effects of charge doping and biaxial strain on the CDW transitions of monolayer 1*T*-TiS_2. Monolayer 1*T*-TiS_2 tends to form a (2×2) CDW superlattice, which can be effectively suppressed by electron doping (ranging from 0.11 to 0.75 e/f.u. under the condition of a vacuum layer of 12 Å). As the electron doping concentration is over 0.76 e/f.u., an unexpected $(\sqrt{7} \times \sqrt{3})$ CDW phase involving a spontaneous breaking of the hexagonal crystal symmetry becomes the ground state. In addition, the dynamic stability of doped monolayer 1*T*-TiS_2 can be tuned by strain. However, neither compressive nor tensile strains alone can stabilize undoped monolayer 1*T*-TiS_2. When decorated by metal atoms, such as Li, Na, K, Ca, and Al, the (2×2) CDW instability can also be suppressed because of electron transfer to the TiS_2 layers. The stable 1*T*-TiS_2 with charge doping or with chemical doping is predicted to exhibit good phonon-mediated superconductivity, which can be further enhanced by strain.

SUPPLEMENTARY MATERIAL

See the supplementary material for phonon dispersions of TiS_2 in the presence of doping and strain, and electronic properties of $Na(TiS_2)_2$ and $NaTiS_2$.

ACKNOWLEDGMENTS

This work was supported by the Guangdong Natural Science Funds for Distinguished Young Scholars (Grant No. 2014A030306024), the National Science Foundation of China (NSFC) (Grant Nos. 11574088, 11704322, and 51706192), the Guangdong Natural Science Funds for Doctoral Program (Grant No. 2017A030310086), and the Shandong Natural Science Funds for Doctoral Program (No. ZR2017BA017). The computations were performed using research computing facilities offered by Information Technology Services, the University of Hong Kong.

REFERENCES

[1]K. S. Novoselov, A. K. Geim, S. V. Morozov, D. Jiang, Y. Zhang, S. V. Dubonos, I. V. Grigorieva, and A. A. Firsov, "Electric field effect in atomically thin carbon films," Science **306**, 666–669 (2004).
[2]S. Cahangirov, M. Topsakal, E. Aktürk, H. Şahin, and S. Ciraci, "Two- and one-dimensional Honeycomb structures of silicon and germanium," Phys. Rev. Lett. **102**, 236804 (2009).
[3]P. Vogt, P. De Padova, C. Quaresima, J. Avila, E. Frantzeskakis, M. C. Asensio, A. Resta, B. Ealet, and G. Le Lay, "Silicene: Compelling experimental evidence for graphenelike two-dimensional silicon," Phys. Rev. Lett. **108**, 155501 (2012).
[4]G. R. Bhimanapati, Z. Lin, V. Meunier, Y. Jung, J. Cha, S. Das, D. Xiao, Y. Son, M. S. Strano, V. R. Cooper, L. Liang, S. G. Louie, E. Ringe, W. Zhou, S. S. Kim, R. R. Naik, B. G. Sumpter, H. Terrones, F. Xia, Y. Wang, J. Zhu, D. Akinwande, N. Alem, J. A. Schuller, R. E. Schaak, M. Terrones, and J. A. Robinson, "Recent advances in two-dimensional materials beyond graphene," ACS Nano **9**, 11509–11539 (2015).
[5]G. Yanfeng, W. Wenhui, Y. Fan, and Y. Yugui, "The strain effect on superconductivity in phosphorene: A first-principles prediction," New J. Phys. **17**, 035008 (2015).
[6]M. Corso, W. Auwärter, M. Muntwiler, A. Tamai, T. Greber, and J. Osterwalder, "Boron nitride nanomesh," Science **303**, 217–220 (2004).
[7]M. Chen, Y.-J. Zhao, J.-H. Liao, and X.-B. Yang, "Transition-metal dispersion on carbon-doped boron nitride nanostructures: Applications for high-capacity hydrogen storage," Phys. Rev. B **86**, 045459 (2012).
[8]J. Zhao, H. Liu, Z. Yu, R. Quhe, S. Zhou, Y. Wang, C. C. Liu, H. Zhong, N. Han, J. Lu, Y. Yao, and K. Wu, "Rise of silicene: A competitive 2D material," Prog. Mater. Sci. **83**, 24–151 (2016).
[9]P. Dang, S. Rouvimov, H. G. Xing, and D. Jena, "Magnetotransport and superconductivity in InBi films grown on Si(111) by molecular beam epitaxy," J. Appl. Phys. **126**, 103901 (2019).
[10]S. Sengupta, E. Tisserond, F. Linez, M. Monteverde, A. Murani, T. Rödel, P. Lecoeur, T. Maroutian, C. Marrache-Kikuchi, A. F. Santander-Syro, and F. Fortuna, "Gate-tunable superconductivity at $SrTiO_3$ surface realized by Al layer evaporation," J. Appl. Phys. **124**, 213902 (2018).
[11]S. Manzeli, D. Ovchinnikov, D. Pasquier, O. V. Yazyev, and A. Kis, "2D transition metal dichalcogenides," Nat. Rev. Mater. **2**, 17033 (2017).
[12]F. Arnold, R.-M. Stan, S. K. Mahatha, H. E. Lund, D. Curcio, M. Dendzik, H. Bana, E. Travaglia, L. Bignardi, P. Lacovig, D. Lizzit, Z. Li, M. Bianchi, J. A. Miwa, M. Bremholm, S. Lizzit, P. Hofmann, and C. E. Sanders, "Novel single-layer vanadium sulphide phases," 2D Mater. **5**, 045009 (2018).
[13]Z. Y. Zeng, C. L. Tan, X. Huang, S. Y. Bao, and H. Zhang, "Growth of noble metal nanoparticles on single-layer TiS_2 and TaS_2 nanosheets for hydrogen evolution reaction," Energy Environ. Sci. **7**, 797–803 (2014).
[14]Y. Z. Ge and A. Y. Liu, "Phonon-mediated superconductivity in electron-doped single-layer MoS_2: A first-principles prediction," Phys. Rev. B **87**, 241408 (2013).
[15]M. Xu, Y. Chen, F. Xiong, J. Wang, Y. Liu, J. Lv, Y. Li, Y. Wang, Z. Chen, and Y. Ma, "A hidden symmetry-broken phase of MoS_2 revealed as a superior photovoltaic material," J. Mater. Chem. A **6**, 16087–16093 (2018).
[16]Y. Zhao, Z. Dai, C. Zhang, C. Lian, S. Zeng, G. Li, S. Meng, and J. Ni, "Intrinsic electronic transport and thermoelectric power factor in n-type doped monolayer MoS_2," New J. Phys. **20**, 043009 (2018).
[17]S. Aas and C. Bulutay, "Geometric band properties in strained monolayer transition metal dichalcogenides using simple band structures," J. Appl. Phys. **126**, 115701 (2019).
[18]T. Habe, "Electronic transmission in the lateral heterostructure of semiconducting and metallic transition-metal dichalcogenide monolayers," J. Appl. Phys. **126**, 123901 (2019).
[19]Z. L. Tao, L. N. Xu, X. L. Gou, J. Chen, and H. T. Yuan, "TiS_2 nanotubes as the cathode materials of Mg-ion batteries," Chem. Commun. **2004**(18), 2080–2081.
[20]A. H. Reshak, I. V. Kityk, and S. Auluck, "Electronic structure and optical properties of 1*T*-TiS_2 and lithium intercalated 1*T*-TiS_2 for lithium batteries," J. Chem. Phys. **129**, 074706 (2008).
[21]Y. P. Liu, H. T. Wang, L. Cheng, N. Han, F. P. Zhao, P. R. Li, C. H. Jin, and Y. G. Li, "TiS_2 nanoplates: A high-rate and stable electrode material for sodium ion batteries," Nano Energy **20**, 168–175 (2016).

[22]S. H. Chung, L. Luo, and A. Manthiram, "TiS_2-polysulfide hybrid cathode with high sulfur loading and low electrolyte consumption for lithium-sulfur batteries," ACS Energy Lett. **3**, 568–573 (2018).
[23]Z. Hu, Z. X. Tai, Q. N. Liu, S. W. Wang, H. L. Jin, S. Wang, W. H. Lai, M. Z. Chen, L. Li, L. N. Chen, Z. L. Tao, and S. L. Chou, "Ultrathin 2D TiS_2 nanosheets for high capacity and long-life sodium Ion batteries," Adv. Energy Mater. **9**, 1803210 (2019).
[24]S. H. Chung and A. Manthiram, "A Li_2S-TiS_2-electrolyte composite for stable Li_2S-based lithium-sulfur batteries," Adv. Energy Mater. **9**, 1901397 (2019).
[25]X. Huang, J. Y. Tang, B. Luo, R. Knibbe, T. G. Lin, H. Hu, M. Rana, Y. X. Hu, X. B. Zhu, Q. F. Gu, D. Wang, and L. Z. Wang, "Sandwich-like ultrathin TiS_2 nanosheets confined within N, S codoped porous carbon as an effective polysulfide promoter in lithium-sulfur batteries," Adv. Energy Mater. **9**, 1901872 (2019).
[26]E. Lee, S. Sahgong, C. S. Johnson, and Y. Kim, "Comparative electrochemical sodium insertion/extraction behavior in layered Na_xVS_2 and Na_xTiS_2," Electrochim. Acta **143**, 272–277 (2014).
[27]L.-P. Zhao, G. Liu, P. Zhang, L.-Q. Sun, L.-N. Cong, W. Lu, Q.-Q. Sun, H.-M. Xie, and H.-Y. Wang, "TiS_2 as negative electrode material for sodium-ion supercapattery," Chem. Pap. **73**, 2583–2589 (2019).
[28]A. Amara, Y. Frongillo, M. J. Aubin, S. Jandl, J. M. Lopez-Castillo, and J.-P. Jay-Gerin, "Thermoelectric power of TiS_2," Phys. Rev. B **36**, 6415–6419 (1987).
[29]H. Imai, Y. Shimakawa, and Y. Kubo, "Large thermoelectric power factor in TiS_2 crystal with nearly stoichiometric composition," Phys. Rev. B **64**, 241104 (2001).
[30]E. Guilmeau, Y. Bréard, and A. Maignan, "Transport and thermoelectric properties in copper intercalated TiS_2 chalcogenide," Appl. Phys. Lett. **99**, 052107 (2011).
[31]C. L. Wan, X. K. Gu, F. Dang, T. Itoh, Y. F. Wang, H. Sasaki, M. Kondo, K. Koga, K. Yabuki, G. J. Snyder, R. G. Yang, and K. Koumoto, "Flexible n-type thermoelectric materials by organic intercalation of layered transition metal dichalcogenide TiS_2," Nat. Mater. **14**, 622–627 (2015).
[32]Y. Zhou, J. Y. Wan, Q. Li, L. Chen, J. Y. Zhou, H. A. Wang, D. R. He, X. R. Li, Y. C. Yang, and H. H. Huang, "Chemical welding on semimetallic TiS_2 nanosheets for high-performance flexible n-type thermoelectric films," ACS Appl. Mater. Interfaces **9**, 42430–42437 (2017).
[33]E. Guilmeau, T. Barbier, A. Maignan, and D. Chateigner, "Thermoelectric anisotropy and texture of intercalated TiS_2," Appl. Phys. Lett. **111**, 133903 (2017).
[34]G. P. Li, K. L. Yao, and G. Y. Gao, "Strain-induced enhancement of thermoelectric performance of TiS_2 monolayer based on first-principles phonon and electron band structures," Nanotechnology **29**, 015204 (2018).
[35]A. Ramakrishnan, S. Raman, L. C. Chen, and K. H. Chen, "Enhancement in thermoelectric properties of TiS_2 by Sn addition," J. Electron. Mater. **47**, 3091–3098 (2018).
[36]K. H. Park, J. Choi, H. J. Kim, D. H. Oh, J. R. Ahn, and S. U. Son, "Unstable single-layered colloidal TiS_2 nanodisks," Small **4**, 945–950 (2008).
[37]Z. Y. Zeng, Z. Y. Yin, X. Huang, H. Li, Q. Y. He, G. Lu, F. Boey, and H. Zhang, "Single-layer semiconducting nanosheets: High-yield preparation and device fabrication," Angew. Chem. Int. Ed. **50**, 11093–11097 (2011).
[38]J. D. Zhou, J. H. Lin, X. W. Huang, Y. Zhou, Y. Chen, J. Xia, H. Wang, Y. Xie, H. M. Yu, J. C. Lei, D. Wu, F. C. Liu, Q. D. Fu, Q. S. Zeng, C. H. Hsu, C. L. Yang, L. Lu, T. Yu, Z. X. Shen, H. Lin, B. I. Yakobson, Q. Liu, K. Suenaga, G. T. Liu, and Z. Liu, "A library of atomically thin metal chalcogenides," Nature **556**, 355–359 (2018).
[39]C. G. Guo, H. Li, W. Zhao, J. Pan, T. Q. Lin, J. J. Xu, M. W. Chen, and F. Q. Huang, "High-quality single-layer nanosheets of MS_2 (M = Mo, Nb, Ta, Ti) directly exfoliated from AMS_2 (A = Li, Na, K) crystals," J. Mater. Chem. C **5**, 5977–5983 (2017).
[40]K. Dolui and S. Sanvito, "Dimensionality-driven phonon softening and incipient charge density wave instability in TiS_2," Europhys. Lett. **115**, 47001 (2016).
[41]M. D. Johannes and I. I. Mazin, "Fermi surface nesting and the origin of charge density waves in metals," Phys. Rev. B **77**, 165135 (2008).
[42]T. Straub, T. Finteis, R. Claessen, P. Steiner, S. Hüfner, P. Blaha, C. S. Oglesby, and E. Bucher, "Charge-density-wave mechanism in 2*H*-$NbSe_2$: Photoemission results," Phys. Rev. Lett. **82**, 4504–4507 (1999).
[43]M. Holt, P. Zschack, H. Hong, M. Y. Chou, and T. C. Chiang, "X-ray studies of phonon softening in $TiSe_2$," Phys. Rev. Lett. **86**, 3799–3802 (2001).
[44]S. V. Borisenko, A. A. Kordyuk, A. N. Yaresko, V. B. Zabolotnyy, D. S. Inosov, R. Schuster, B. Büchner, R. Weber, R. Follath, L. Patthey, and H. Berger, "Pseudogap and charge density waves in two dimensions," Phys. Rev. Lett. **100**, 196402 (2008).
[45]K. Rossnagel, "On the origin of charge-density waves in select layered transition-metal dichalcogenides," J. Phys. Condens. Matter **23**, 213001 (2011).
[46]J. A. Wilson, F. J. Di Salvo, and S. Mahajan, "Charge-density waves and superlattices in the metallic layered transition metal dichalcogenides," Adv. Phys. **24**, 117–201 (1975).
[47]J. Dai, E. Calleja, J. Alldredge, X. Zhu, L. Li, W. Lu, Y. Sun, T. Wolf, H. Berger, and K. McElroy, "Microscopic evidence for strong periodic lattice distortion in two-dimensional charge-density wave systems," Phys. Rev. B **89**, 165140 (2014).
[48]P. Chen, W. W. Pai, Y. H. Chan, A. Takayama, C. Z. Xu, A. Karn, S. Hasegawa, M. Y. Chou, S. K. Mo, A. V. Fedorov, and T. C. Chiang, "Emergence of charge density waves and a pseudogap in single-layer $TiTe_2$," Nat. Commun. **8**, 516 (2017).
[49]B.-T. Wang, P.-F. Liu, J.-J. Zheng, W. Yin, and F. Wang, "First-principles study of superconductivity in the two- and three-dimensional forms of $PbTiSe_2$: Suppressed charge density wave in 1*T*-$TiSe_2$," Phys. Rev. B **98**, 014514 (2018).
[50]J. Feng, D. Biswas, A. Rajan, M. D. Watson, F. Mazzola, O. J. Clark, K. Underwood, I. Marković, M. McLaren, A. Hunter, D. M. Burn, L. B. Duffy, S. Barua, G. Balakrishnan, F. Bertran, P. Le Fèvre, T. K. Kim, G. van der Laan, T. Hesjedal, P. Wahl, and P. D. C. King, "Electronic structure and enhanced charge-density wave order of monolayer VSe_2," Nano Lett. **18**, 4493–4499 (2018).
[51]C. S. Lian, C. Si, J. Wu, and W. H. Duan, "First-principles study of Na-intercalated bilayer $NbSe_2$: Suppressed charge-density wave and strain-enhanced superconductivity," Phys. Rev. B **96**, 235426 (2017).
[52]A. Y. Liu, "Electron-phonon coupling in compressed 1*T*-TaS_2: Stability and superconductivity from first principles," Phys. Rev. B **79**, 220515 (2009).
[53]L.-Y. Gan, L.-H. Zhang, Q. Zhang, C.-S. Guo, U. Schwingenschlögl, and Y. Zhao, "Strain tuning of the charge density wave in monolayer and bilayer 1*T*-TaS_2," Phys. Chem. Chem. Phys. **18**, 3080–3085 (2016).
[54]C.-S. Lian, C. Si, and W. Duan, "Unveiling charge-density wave, superconductivity, and their competitive nature in two-dimensional $NbSe_2$," Nano Lett. **18**, 2924–2929 (2018).
[55]M. M. Ugeda, A. J. Bradley, Y. Zhang, S. Onishi, Y. Chen, W. Ruan, C. Ojeda-Aristizabal, H. Ryu, M. T. Edmonds, H.-Z. Tsai, A. Riss, S.-K. Mo, D. Lee, A. Zettl, Z. Hussain, Z.-X. Shen, and M. F. Crommie, "Characterization of collective ground states in single-layer $NbSe_2$," Nat. Phys. **12**, 92–97 (2016).
[56]B. Guster, E. Canadell, M. Pruneda, and P. Ordejón, "First principles analysis of the CDW instability of single-layer 1*T*-$TiSe_2$ and its evolution with charge carrier density," 2D Mater. **5**, 025024 (2018).
[57]P. Chen, W. W. Pai, Y. H. Chan, V. Madhavan, M. Y. Chou, S. K. Mo, A. V. Fedorov, and T. C. Chiang, "Unique gap structure and symmetry of the charge density wave in single-layer VSe_2," Phys. Rev. Lett. **121**, 196402 (2018).
[58]L. Liu and H. L. L. Zhuang, "Tunable phase transition in single-layer $TiSe_2$ via electric field," J. Solid State Chem. **262**, 309–312 (2018).
[59]Z. G. Fu, J. H. Wang, Y. Yang, W. Yang, L. L. Liu, Z. Y. Hu, and P. Zhang, "Doping stability and charge-density-wave transition of strained 1*T*-$TiSe_2$," Europhys. Lett. **120**, 17006 (2017).
[60]S. Fragkos, R. Sant, C. Alvarez, A. Bosak, P. Tsipas, D. Tsoutsou, H. Okuno, G. Renaud, and A. Dimoulas, "Room temperature commensurate charge density wave in epitaxial strained $TiTe_2$ multilayer films," Adv. Mater. Int. **6**, 1801850 (2019).

[61]B. Guster, R. Robles, M. Pruneda, E. Canadell, and P. Ordejón, "2 × 2 charge density wave in single-layer $TiTe_2$," 2D Mater. **6**, 015027 (2019).
[62]D. S. Inosov, V. B. Zabolotnyy, D. V. Evtushinsky, A. A. Kordyuk, B. Büchner, R. Follath, H. Berger, and S. V. Borisenko, "Fermi surface nesting in several transition metal dichalcogenides," New J. Phys. **10**, 125027 (2008).
[63]X. X. Xi, L. Zhao, Z. F. Wang, H. Berger, L. Forró, J. Shan, and K. F. Mak, "Strongly enhanced charge-density-wave order in monolayer $NbSe_2$," Nat. Nanotechnol. **10**, 765–769 (2015).
[64]Y. S. Wu, J. M. He, J. Y. Liu, H. Xing, Z. Q. Mao, and Y. Liu, "Dimensional reduction and ionic gating induced enhancement of superconductivity in atomically thin crystals of 2*H*-$TaSe_2$," Nanotechnology **30**, 035702 (2019).
[65]X. X. Xi, Z. F. Wang, W. W. Zhao, J. H. Park, K. T. Law, H. Berger, L. Forró, J. Shan, and K. F. Mak, "Ising pairing in superconducting $NbSe_2$ atomic layers," Nat. Phys. **12**, 139–143 (2016).
[66]Y. Liu, L. J. Li, W. J. Lu, R. Ang, X. Z. Liu, and Y. P. Sun, "Coexistence of superconductivity and commensurate charge density wave in 4H_b-$TaS_{2-x}Se_x$ single crystals," J. Appl. Phys. **115**, 043915 (2014).
[67]Y. Liu, W. J. Lu, L. J. Li, X. D. Zhu, W. H. Song, R. Ang, L. S. Ling, X. Z. Liu, and Y. P. Sun, "Tuning the charge density wave and superconductivity in 6*R*-$TaS_{2-x}Se_x$," J. Appl. Phys. **117**, 163912 (2015).
[68]L. J. Li, E. C. T. O'Farrell, K. P. Loh, G. Eda, B. Özyilmaz, and A. H. Castro Neto, "Controlling many-body states by the electric-field effect in a two-dimensional material," Nature **529**, 185–189 (2016).
[69]P. Giannozzi, S. Baroni, N. Bonini, M. Calandra, R. Car, C. Cavazzoni, D. Ceresoli, G. L. Chiarotti, M. Cococcioni, I. Dabo, A. Dal Corso, S. de Gironcoli, S. Fabris, G. Fratesi, R. Gebauer, U. Gerstmann, C. Gougoussis, A. Kokalj, M. Lazzeri, L. Martin-Samos, N. Marzari, F. Mauri, R. Mazzarello, S. Paolini, A. Pasquarello, L. Paulatto, C. Sbraccia, S. Scandolo, G. Sclauzero, A. P. Seitsonen, A. Smogunov, P. Umari, and R. M. Wentzcovitch, "QUANTUM ESPRESSO: A modular and open-source software project for quantum simulations of materials," J. Phys. Condens. Matter **21**, 395502 (2009).
[70]P. E. Blöchl, "Projector augmented-wave method," Phys. Rev. B **50**, 17953–17979 (1994).
[71]J. P. Perdew, K. Burke, and M. Ernzerhof, "Generalized gradient approximation made simple," Phys. Rev. Lett. **77**, 3865–3868 (1996).
[72]N. Marzari, D. Vanderbilt, A. De Vita, and M. C. Payne, "Thermal contraction and disordering of the Al(110) surface," Phys. Rev. Lett. **82**, 3296–3299 (1999).
[73]H. J. Monkhorst and J. D. Pack, "Special points for Brillouin-zone integrations," Phys. Rev. B **13**, 5188–5192 (1976).
[74]M. J. Wei, W. J. Lu, R. C. Xiao, H. Y. Lv, P. Tong, W. H. Song, and Y. P. Sun, "Manipulating charge density wave order in monolayer 1*T*-$TiSe_2$ by strain and charge doping: A first-principles investigation," Phys. Rev. B **96**, 165404 (2017).
[75]E. B. Isaacs and C. A. Marianetti, "Electronic correlations in monolayer VS_2," Phys. Rev. B **94**, 035120 (2016).
[76]P. B. Allen and R. C. Dynes, "Transition temperature of strong-coupled superconductors reanalyzed," Phys. Rev. B **12**, 905–922 (1975).
[77]Y. Zhao, S. Zeng, and J. Ni, "Phonon-mediated superconductivity in borophenes," Appl. Phys. Lett. **108**, 242601 (2016).
[78]E. S. Penev, A. Kutana, and B. I. Yakobson, "Can two-dimensional boron superconduct?" Nano Lett. **16**, 2522–2526 (2016).
[79]J.-H. Liao, Y.-C. Zhao, Y.-J. Zhao, H. Xu, and X.-B. Yang, "Phonon-mediated superconductivity in Mg intercalated bilayer borophenes," Phys. Chem. Chem. Phys. **19**, 29237–29243 (2017).
[80]S. Zeng, Y. Zhao, G. Li, and J. Ni, "Strongly enhanced superconductivity in doped monolayer MoS_2 by strain," Phys. Rev. B **94**, 024501 (2016).
[81]J.-J. Zhang, B. Gao, and S. Dong, "Strain-enhanced superconductivity of MoX_2 (X = S or Se) bilayers with Na intercalation," Phys. Rev. B **93**, 155430 (2016).
[82]Y. C. Zhao, S. M. Zeng, C. Lian, Z. H. Dai, S. Meng, and J. Ni, "Multigap anisotropic superconductivity in borophenes," Phys. Rev. B **98**, 134514 (2018).
[83]Y. Sun, J. Lv, Y. Xie, H. Liu, and Y. Ma, "Route to a superconducting phase above room temperature in electron-doped hydride compounds under high pressure," Phys. Rev. Lett. **123**, 097001 (2019).
[84]G. Henkelman, A. Arnaldsson, and H. Jónsson, "A fast and robust algorithm for Bader decomposition of charge density," Comput. Mater. Sci. **36**, 354–360 (2006).